PERGAMON

Available online at www.sciencedirect.com
SCIENCE DIRECT®

Planetary and Space Science 51 (2003) 339–352

Planetary and Space Science

www.elsevier.com/locate/pss

Solar energetic particle event at Mercury

F. Leblanc[a,*], J.G. Luhmann[b], R.E. Johnson[c], M. Liu[c]

[a] *Service d'Aéronomie du CNRS, B.P. No. 3, Verrières-Le-Buisson 91371, France*
[b] *Space Science Laboratory, University of California, Berkeley, USA*
[c] *University of Virginia, Charlottesville, USA*

Received 23 April 2002; accepted 3 December 2002

Abstract

Mercury's magnetosphere only partially protects its surface from solar particles. When a solar energetic particle (SEP) event encounters Mercury, a significant flux of energetic particles will reach Mercury's surface which can change Mercury's exosphere. In this paper, we describe some of the consequences of the encounter of a SEP event with Mercury before and few hours after the shock associated with such an event reaches Mercury. Energetic ions and electrons with energy between 10 keV and 10 MeV are followed across a model of Mercury's magnetosphere (J. Geophys. Res. 103 (1998) 9113). The effects of such an encounter on the ion and neutral exospheres are estimated for one particular gradual proton event reported by Reames et al. (Astrophys. J. 483 (1997a) 515) and scaled to Mercury's orbit. After the arrival of these SEP at Mercury, a population of quasi-trapped energetic ions and electrons is expected close to Mercury which is stable for hours after their arrival at Mercury. A significant dawn/dusk charge separation is observed. A fraction of the initial energetic particles ($\sim 10\%$) impact the surface with a spatial distribution that exhibits north/south and dawn/dusk asymmetries. The flux of particles impacting the surface and the ability of a quasi-trapped population to be maintained near Mercury are highly dependent on the Bz sign of the interplanetary magnetic field. The impacting SEP can eject a non-uniform distribution of sodium atoms into Mercury's exosphere and can be the origin of several exospheric features observed during last decade.

Keywords: Mercury; Space weather; Magnetosphere; Exosphere; Sputtering; Sodium

1. Introduction

The only observations of Mercury magnetosphere were obtained 30 years ago by Mariner 10 during three flybys. Despite this small number of observations, it is now generally believed that Mercury does have an intrinsic magnetosphere (Ness et al., 1974). This is the case despite its size, its slow sidereal rotation and its tectonically dead surface like that of the Moon. Another surprising observation by Mariner 10 was the existence of bursts of electron and proton with energy up to 600 keV (Simpson et al., 1974). These were first attributed to magnetospheric mechanisms of acceleration like Earth substorm (Siscoe et al., 1975; Eraker and Simpson, 1986; Baker et al., 1986) or to energetic Jovian electrons trapped inside the Hermean magnetosphere (Baker, 1986). However Mercury's magnetosphere has been shown to be highly dynamic compared to the Earth's magnetosphere in particular with respect to the interplanetary magnetic field (IMF). Therefore, such variations could be at the origin of the observed energetic electrons bursts (Luhmann et al., 1998). Unfortunately, during the flybys of Mariner 10, no other plasma observation were obtained. UV spectroscopy on board Mariner 10 measured the neutral environment of Mercury. Three elements were identified: H, He and O (Broadfoot et al., 1976) with a total density at the subsolar point of less than 10^6 particles/cm^3. Mercury's neutral atmosphere is, therefore, fully non-collisional. That is, it is an exosphere.

Most of the observations of Mercury's neutral exosphere have been made from the Earth. These observations have revealed the presence of sodium atoms (Potter and Morgan, 1985), of potassium atoms (Potter and Morgan, 1986) and of calcium atoms (Bida et al., 2000). Several of the observations of Mercury's sodium exosphere have provided important information on its origins. Temporal variations of Mercury sodium exosphere have been observed with respect to Mercury's position (Potter and Morgan, 1987) and on time scale much smaller than Mercury's day (Potter and Morgan, 1990; Potter et al., 1999). Spatial inhomo-

* Corresponding author.
E-mail address: francois.leblanc@aerov.jussieu.fr (F. Leblanc).

0032-0633/03/$ - see front matter © 2003 Elsevier Science Ltd. All rights reserved.
doi:10.1016/S0032-0633(02)00207-6

geneities on Mercury's dayside sodium exosphere have been reported (Sprague et al., 1997; Potter et al., 1999). All these observations indicate that several distinct processes produce Mercury sodium exosphere. In order of importance following Killen and Ip (1999), these processes are photo stimulated and thermal desorptions (McGrath et al., 1986; Madey et al., 1998), sputtering by impacting energetic particles (Potter and Morgan, 1997; Killen et al., 2001), micro-meteoritic vaporization (Morgan et al., 1988; Hunten et al., 1988; Cintala, 1992; Langevin, 1997) and chemical sputtering (Potter, 1995). Most of these processes generate different energy distributions for the particle ejected from the surface and have different spatial distributions at the surface of Mercury. Sputtering is mainly due to solar particles which penetrate Mercury's magnetosphere along open magnetic field lines most often at high latitudes (Kabin et al., 2000; Killen et al., 2001; Sarrantos et al., 2001). Photo stimulated and thermal desorptions are due to solar photons impacting the surface on the dayside. Micro-meteoritic bombardment is more important on the dawn side than on the dusk side (Killen and Ip, 1999). Potter and Morgan (1990) and Potter et al. (1999) have observed strong emission enhancements at high latitudes which have been suggested to correlate with solar particle sputtering (Killen et al., 2001), whereas significant differences between morning and afternoon emission brightnesses suggest exospheric sodium production dominated by photo stimulated and thermal desorptions (Sprague et al., 1997). In order to fully describe the sodium exosphere, the sinks have also to be considered. These sinks are mainly neutral loss by escape enhanced by the solar pressure acceleration (Smyth, 1986), thermalization at the surface (Shemansky and Broadfoot, 1977; Hunten and Sprague, 1997) and solar photo-ionization of exospheric neutral particles which are then accelerated out of Mercury's magnetosphere by the electric field of convection associated with the solar wind (Ip, 1987). These loss processes are dependent on Mercury's position with respect to the Sun as observed by Potter and Morgan (1987). Another key parameter for understanding the origins of the sodium exosphere is the high variability of Mercury's magnetosphere (Luhmann et al., 1998), in particular with respect to the IMF orientation. Indeed it significantly affects the ability of solar particles to reach Mercury's surface (Killen et al., 2001; Sarrantos et al., 2001).

In this paper, we describe another temporal effect which acts on Mercury's exosphere: the encounter of a solar energetic particles (SEP) event and Mercury before and few hours after the shock associated with such an event reaches Mercury. This situation was initially suggested to be the origin of the enhancements in the sodium exosphere observed by Potter et al. (1999). In order to describe such an encounter, we consider a SEP event observed at the Earth (Reames et al., 1997a) that we rescale to Mercury's orbit. The different ion species which compose this event, H^{+}, He^{2+}, C^{6+}, O^{7+} and Fe^{12+}, are followed inside Mercury's magnetosphere. For electrons, we consider a different event reported by Simnett (1974). Our approach has no statistical aim and is developed in order to be able to scale the effects due to the encounter of a SEP event with Mercury.

As a first step, we estimate the strength of the electric field of convection associated with the solar wind and the capability of incident particles to penetrate the magnetic field pile up of the IMF in the magnetosheath. In this paper, we scale a model of Mars' magnetosheath (Luhmann et al., 2002) to Mercury and estimate for which energy an incident particle could be significantly influenced inside Mercury's magnetosheath.

Mercury's magnetosphere is poorly known, but can reasonably be considered as a scaled version of the Earth's magnetosphere (Ogilvie et al., 1977). It has been successfully described by Luhmann et al. (1998) who used a scaled version of a databased model of the Earth's magnetosphere (Tsyganenko, 1996). We follow test-particles inside this model of the magnetosphere until they either leave the magnetosphere or impact the surface. We deduce the lifetime and position of SEP inside Mercury's magnetosphere after injection. The intensity, energy and spatial distributions of the flux of particles impacting the surface is calculated. The total number of ejected sodium neutral atoms from the surface due to this flux is then estimated. These results suppose that Mercury's magnetosphere for quiet solar wind conditions (Luhmann et al., 1998) is not significantly changed by the SEP event. Our study is therefore willingly restrained to the time during which the shock associated with such event does not pertubate Mercury's magnetosphere.

In Section 2, we present the SEP event used for this work (Section 2.1) and describe the SEP inside Mercury's magnetosheath (Section 2.2) and inside Mercury's magnetosphere (Section 2.3). In Section 3, we describe the consequences of the encounter of this SEP event with Mercury. The flux reaching the surface is provided in Section 3.1. The lifetime and position of the particles inside the magnetosphere are given in Section 3.2. In Section 3.3, the role of the IMF orientation is underlined. Since energetic particles can both sputter and cause enhanced diffusion of sodium atoms (McGrath et al., 1986), we estimate the total number of sodium atoms ejected from the surface in Section 3.4. The conclusions are given in Section 4.

2. Solar energetic particle and Mercury

2.1. Solar energetic particle event

SEP events are divided into two groups (Reames, 1999): the impulsive flare events (IFE) which are composed of energetic particles accelerated at the base of the solar corona in association with flare eruptions and the gradual proton events (GPE) which are composed of energetic particles accelerated by coronal mass ejection (CME) from the corona up to several solar radii (Kahler et al., 1984). Both events

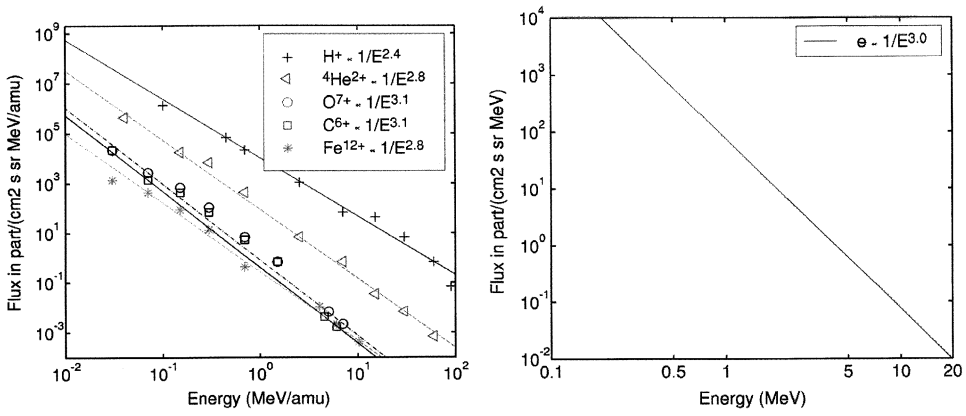

Fig. 1. SEP event rescaled to Mercury's orbit. (a) Gradual proton event of 1995 October 20 as reported by Reames et al. (1997a), Flux of H^{+}, He^{2+}, C^{6+}, O^{7+} and Fe^{12+}. (b) Flux of electrons associated with a SEP event of 1968 September 30 (Fig. 15 in Simnett, 1974). The lines are power law fit and symbols in Fig. 1a are measurements reported by Reames et al. (1997a). Values of the power law fit are indicated on each figure.

are associated with similar population in terms of ion and energy range but are significantly different in terms of charge state, spatial and temporal distributions and flux intensities (Reames, 1995). GPE have larger flux and distribution in helio-longitude than IFE. Moreover, GPE can last up to 2–3 days (Reames et al., 1997b) whereas IFE last only few hours (Reames, 1995). However IFE are much more frequent than GPE: in solar maximum period up to 100 IFE are observed per year at the Earth whereas only 10 GPE are observed. In this work, we will consider the particular case of a GPE reported by Reames et al. (1997a). These results can then be extrapolated to most IFE and GPE taking into account the differences in flux from the event we used.

The GPE reported by Reames et al. (1997a) is a quite well detailed observation of high flux of energetic ions with a time invariant power law distribution of energy during $\sim$ 3 days (Fig. 1 for ions). For electrons (Fig. 1), we use an event reported by Simnett et al. (1974) since no electron measurements for the event reported by Reames et al. (1997a) are available. To use two different SEP events to describe the effects of energetic ions and electrons on Mercury is valid since we study each species separately and neglect interactions between these particles near Mercury. However, the ratio between the flux of ions and electrons is consistent with the observations that GPE are electron poor events (Reames, 1995). The part of the SEP event considered in this study for the ion is composed of particles with energy between 10 keV/amu to 100 Mev/amu (Fig. 1 for ion). The ion charge state (see legend in Fig. 1 for ion) is deduced from Oetlicker et al. (1997) and is close to the average ion charge state of solar wind particles (Von Steiger et al., 2000). Theory of the acceleration of GPE (Lee, 1997), observations (Gosling et al., 1981) and models (Ellison and Ramaty, 1985; Lee, 1997; Baring et al., 1997) predict that their flux should follow a power law in energy as shown in Fig. 1 for ion. This power law distribution is valid up to a particular energy threshold, which depends on the shock at the origin of the acceleration (Ellison and Ramaty, 1985), down to solar wind energy ($\sim$ 1 keV/amu).

We will limit our study to the energies above 10 keV/amu. First of all, transport effects limit significantly the intensity of the flux at low energy with respect to a power law extrapolation from measurements around MeV/amu (Tylka, 2001). Secondly, SEP of a GPE with energy below 10 keV/amu would roughly encounter Mercury in the same time interval as the shock associated with the GPE. The shock and magnetic cloud (Burlaga, 1991) should significantly change Mercury's magnetosphere (Goldstein et al., 1981) such that our model of Mercury's magnetosphere for quiet solar wind period is not valid. Moreover, solar particles with an energy smaller than 10 keV/amu are significantly affected by the convective electric field of the solar wind inside the magnetosphere and inside the magnetosheath as it will be shown in the next section.

2.2. *Solar particle inside Mercury's magnetosheath*

In a first step, we estimate the strength of the convective electric field associated with the solar wind and of the solar wind magnetic field pile up in the magnetosheath to deflect incident solar particles. This is done by calculating the energy above which the spatial and energy distributions of the incident solar energetic particles at the bow shock are not significantly changed across the magnetosheath down to the magnetopause. We adapt a model used for Mars (Leblanc et al., 2002) to the case of Mercury. This model describes the draping of the solar wind magnetic field lines around a non-magnetized planet and has been developed from a 3D magnetohydrodynamic approach successfully tested for Mars and Venus (Luhmann et al., 2002). We rescale the IMF intensity to the one at Mercury (which consists of

multiplying by a factor five), consider the same slow solar wind velocity (400 km/s) and scale the size of the obstacle to the size of Mercury's magnetosphere. The IMF is fixed to $(0,-10,-10$ nT) for the purposes of the initial calculations that is perpendicular to the Sun–Mercury axis. The average IMF intensity observed by Mariner 10 close to Mercury was equal to 20 nT. The Parker spiral magnetic field forms an angle of $\sim 20^\circ$ with the solar wind direction. The orientation of the IMF perpendicular to the solar wind direction used in this section has been shown in the case of Mars to generate the strongest barrier for solar wind particle to penetrate the magnetosheath (Brecht, 1997). This will given an upper limit to the influence of the convective electric field and magnetic pile up barrier against penetration.

This model is far from being a correct description of the draping of the solar wind magnetic field lines around Mercury (in particular of the magnetic field pile up). It gives, however, a useful indication of the importance of the solar magnetic field pile up in the magnetosheath and of the solar wind convective electric field on the trajectories of incident solar particles.

Test-particles are launched from the bow shock. The bow shock is defined as a conic surface with an axis of symmetry along the Sun–Mercury line and a subsolar point at 1495 km from the surface (Luhmann et al., 1998): that is by the relation $r = L/(1 + \mathrm{e}\cos\theta)$ where r is the distance between Mercury's center and the point on the bow shock and θ is the angle from the Sun–Mercury axis (the X-axis). L is equal to 2.5 Mercury's radii (R_M) and e=0.55. Test-particles for the five species (Fig. 1a) and for the electron (Fig. 1b) are launched from the subsolar point up to $2R_M$ tailward. We study an energy range between 1 and 50 keV/amu and deduce the initial velocity vector for each particle from a truncated isotropic velocity distribution with an average velocity towards Mercury's magnetosphere. Each particle is weighted by a value which is equal to the product of the flux per cm^2/s at the energy of the particle (Fig. 1a) times a constant area. This area is part of the total surface of a flat section placed perpendicularly to the Sun–Mercury line. The flux of solar particles across this section is supposed uniform and at the bow shock is calculated from the projection on the bow shock of this section. Test-particles move in a magnetic field with a time step defined as less than 0.5% of the local gyroperiod (value optimized for computing time and accuracy constraints) until either such particle reaches the magnetopause or bow shock again. The final spatial and energy distributions of the particles impacting the magnetopause are then calculated. By comparing these distributions with the initial ones at the bow shock, we then deduce above which energy a SEP crosses the magnetosheath without being significantly influenced.

Fig. 2 compares the energy flux distribution of H^+ ions at Mercury's bow shock with the energy flux distribution at the magnetopause. $\sim 30,000$ test-particles have been used to obtain this result: the energy being divided into 10 intervals and the surface of the section perpendicular to the Sun–Mercury line into ~ 3000 equal areas. The energy distribution shown Fig. 2 is the total flux reaching the surface averaged over the whole bombarded surface. The energy distribution at the bow shock is presented in Fig. 1a (solid cross line). As shown in Fig. 2, above 5 keV, the energy flux distribution of H^+ ions is not significantly changed across the magnetosheath. We apply the same method for all the species and found that the energy flux distribution of the incident ions is not changed above 8 keV/amu and above 10 keV for electrons. The spatial distribution of the particles at the magnetopause is also not different above this energy from the one at the bow shock.

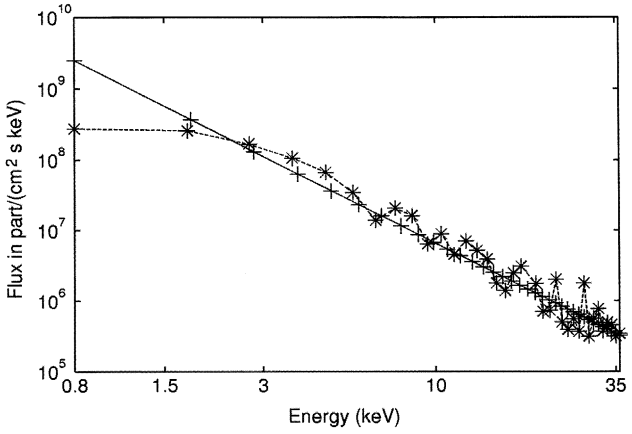

Fig. 2. Flux of H^+ SEP. Solid cross line: initial flux at the bow shock (same than solid cross line in Fig. 1a). Dashed star line: flux of H^+ ion at Mercury's magnetopause.

At an energy of 1 keV/amu, that is for solar wind energies, the flux of the H^+ ions reaching the magnetopause is decreased by one order of magnitude compared to the initial flux at the bow shock (Fig. 2). The flux of solar wind particles impacting Mercury's surface is, therefore, probably less than the product of the surface of open magnetic field lines of Mercury's magnetosphere at the magnetopause times the solar wind flux. The Tsyganenko 96 model approximates open field line regions using an IMF-dependent penetrating field description. However, here we make no attempt to modify and join the magnetosheath model inner boundary to the magnetosphere model boundary, which would be difficult to do with any physical realism. Eventually, these types of calculations should be carried out using the magnetic and electric fields from an MHD simulation of the solar wind interaction with Mercury (e.g. Kabin et al., 2000).

2.3. *Solar energetic particle inside Mercury's magnetosphere*

The second step of this study is to describe how test-particles launched at the magnetopause move inside the magnetosphere. Mercury's magnetosphere described by

Luhmann et al. (1998) is a scaled version of a databased model for the Earth's magnetosphere (Tsyganenko, 1996). This databased model has been constructed from the measurement of currents inside the Earth's magnetosphere from which the induced magnetic fields are calculated: the Earth dipole, the Birkeland region 1 and 2 currents, the tail current, the ring current and the magnetopause current. However, because of the volume occupied by Mercury's planet inside its own magnetosphere, Luhmann et al. (1998) suppressed the contribution due to the ring current. Scale laws to adapt Tsyganenko's model to the case of Mercury are a spatial scale reducing the hermean magnetosphere by a factor seven and a scale factor equal to two increasing the intensity of Mercury's magnetic dipole. Luhmann et al. (1998) have shown that their model gives a good agreement with Mariner 10 observations taking into account the significant variation of the magnetosphere with respect to the IMF orientation. This model is one possible description of Mercury's magnetosphere (Sarrantos et al., 2001; Kabin et al., 2000; Delcourt et al., 2002) and we will discuss further how some of its characteristics affects our conclusions.

Each SEP species is represented by $\sim$ 400,000 test-particles in the range of energy between 10 keV/amu (100 keV for the electrons) to 15 MeV. The energy range is divided into 100 intervals. For each one $\sim$ 4000 test-particles are launched at the magnetopause in order to cover the magnetopause from the subsolar point at $\sim$ 700 km from the surface up to distance of $2R_M$ tailward. The magnetopause is represented by the same type of conic surface as for the bow shock (Section 2.2) with $L = 2R_M$. Each test-particle is weighted by a value equal to the flux at its initial energy (Fig. 1) times a small area of a flat section perpendicular to the Sun–Mercury line. The spatial distribution of the test-particles at the magnetopause is defined and calculated in the same way as described in Section 2.2. Their initial velocity distribution is a truncated isotropic distribution as in section 2.2. Each particle is followed inside the magnetosphere until either it impacts the surface or crosses the magnetopause one more time. The motion of each particle is calculated by solving the equation of motion for a time step defined as the minimum between a fraction of the local gyroradius (typically less than 1%) and the time for each particle to make less than a fraction of Mercury radius (typically less than 1/1000). This time step has been optimized for accuracy and computing time constraints. In order to treat electrons at MeV energies, a relativistic correction to the equation of motion has been added.

Fig. 3 displays examples of trajectories of test-particles launched from the magnetopause and which impact the surface. The $+X$ direction is towards the Sun and the $+Z$-axis is the direction of the rotation vector of Mercury. The stars indicate the launched positions at the magnetopause, the dots the positions of the impact at Mercury's surface, gray lines are the trajectories of each particle and the dark lines

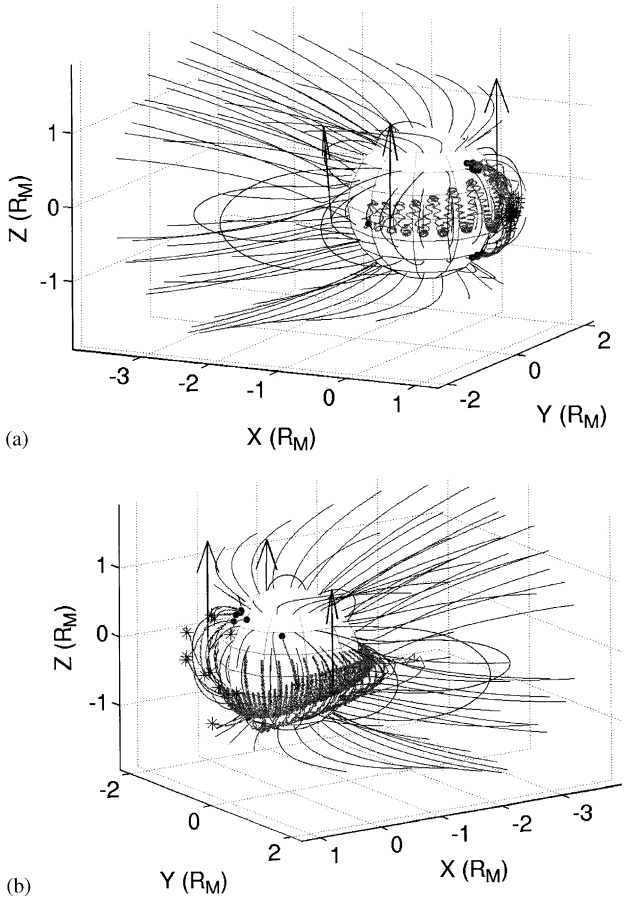

Fig. 3. Trajectories from Mercury's magnetopause of particle impacting Mercury's surface. (a) 20 trajectories of H^+ ion with 10 keV initial energy at the magnetopause. (b) 12 trajectories of electron with 100 keV initial energy at the magnetopause. Solid thin lines: magnetic field lines of Mercury's magnetosphere. Arrows: direction of the magnetic field. Stars: initial position of the particles at the magnetopause. Dots: final position of the particles at the surface. Clear thick line: trajectories of the particles. The sun is in the $+X$ direction.

are the magnetic field lines of Mercury's magnetosphere. The arrows indicate the orientation of Mercury's magnetic field at a few points on the equator. The magnetosphere shown in Fig. 3 has been obtained for an IMF equal to $(0, -10, -10$ nT).

As shown in Fig. 3, there are essentially two types of trajectory for a particle to reach the surface: the trajectory along open magnetic field lines and the trajectory across closed magnetic field lines. In the later case, test-particles are quasi-trapped inside the magnetosphere and move azimuthally towards the terminator. Their motion is mainly driven by the $qv \times B_{\text{Mercury}}$ force (q is the charge of the particle and v its velocity in Mercury's reference frame) and, therefore, leads to charge dependent spatial distribution inside the magnetosphere of Mercury. In the present case of Mercury's dipole field orientation, ions are driven towards the dawn side whereas electrons are driven towards the dusk side. As shown in Fig. 3, ion gyroradii are of the order

of Mercury's radius whereas electron gyroradii are much smaller than Mercury's radius. As a consequence, electrons are impacting the surface at the footprints of the magnetic field lines where they enter the magnetosphere at the magnetopause (that is preferentially at high latitudes) whereas ions are impacting the surface with a large dispersion in latitude.

2.4. Encounter of a SEP event with Mercury

As stated in the introduction, the use of a scaled version of a Earth's model (Tsyganenko, 1996) validated for Mercury's magnetosphere by Luhmann et al. (1998) for quiet solar wind conditions implies that we do not consider the potential effects of the SEP event on Mercury's magnetosphere. Therefore, our study is restrained to the time during which the shock associated with the GPE does not change significantly Mercury's magnetosphere. The shock associated with this GPE was observed at the Earth during few hours whereas the large flux of energetic particles described Fig. 1 were observed during few days (Reames et al., 1997a)

2.5. Flux at the surface

Fig. 4a presents the spatial distribution at the surface of the flux of impacting H^+ particles for an initial flux at the magnetopause as presented in Fig. 1a (solid cross line) within the energy range from 10 keV to 10 MeV. This result has been obtained from $\sim 400,000$ test-particle and for an IMF vector $(0,-10,-10\ \mathrm{nT})$ (Fig. 3). Fig. 4a shows that the flux impacting the surface is not only restricted to the regions with open magnetic field lines as usually supposed for solar wind particles (Killen et al., 2001). The impact distribution at the surface is significant at the equator and is elongated towards dawn longitude. Actually the $qv \times B_{\mathrm{Mercury}}$ force favors the motion of an ion towards the surface on the dawn side and pushes it away from the surface on the dusk side. This force has an opposite effect on the electron (Fig. 4b). This force is at the origin of the significant higher flux of ions reaching the dawn side than the one reaching the dusk side. Another source of asymmetry of the incident flux was also partially described by Ip (1993) and in more detail by Delcourt et al. (2003) for sodium ions created in the magnetotail with more than 10 keV energy and reimpacting the surface of Mercury with a similar dawn/dusk asymmetric distribution on the nightside (but here because of the gradient B drift effect). The $qv \times B_{\mathrm{Mercury}}$ force is less efficient for generating a dawn/dusk asymmetry of the electron flux impacting the surface because the electron gyroradius inside Mercury's magnetosphere is only of few km. The asymmetry distribution of the impacting flux is due to particles which have large enough gyroradius (that is enough energy) to penetrate deep inside closed magnetic field loops and move azimuthally towards the terminator. It is, therefore, dependent on the structure of the closed magnetic field lines. A less compressed Mercury's magnetosphere, corresponding to a larger volume of closed magnetic field lines, is possible in the case of a smaller solar wind pressure and would lead to an even larger dispersion of the impacts at Mercury's surface than described in Fig. 4.

We repeat this work for the four other ion species considered in Fig. 1a and find the same characteristics for the flux impacting the surface. Only 8% of the incident H^+ ions, which could have reached the surface if no magnetosphere was there, reach the surface, whereas 11% of the incident He^{2+}, C^{6+}, O^{7+} and Fe^{12+} reach the surface for the same energy range. This is due to the smaller gyroradius of an H^+ than the gyroradii of He^{2+}, C^{6+}, O^{7+} and Fe^{12+}. For an IMF $(0,-10,-10\ \mathrm{nT})$ and the initial flux of SEP shown Fig. 1a, we found that 8×10^{24} H^+/s, 3×10^{23} He^{2+}/s, 2×10^{22} O^{7+}/s, 8×10^{21} C^{6+}/s and 2×10^{21} Fe^{12+}/s reach the surface. For the initial flux of electron shown Fig. 1b, we found that 6×10^{21} electrons/s reach Mercury's surface. These value can be compared to the 1.4×10^{27} solar wind particles/s which following Killen et al. (2001) impact Mercury's surface during the period of the observations of Potter et al. (1999). Their estimate were however made for 1 keV/amu particles with unusual strong intensity of the solar wind flux (that is around 4×10^9 1 keV $H^+/cm^2/s$ at the bow shock with respect to the flux of 10^6 10 keV $H^+/cm^2/s$ that we consider here). These authors also neglected all screening effects as described in the previous section due to the magnetosheath and solar wind electric field of convection. We made the same calculation for H^+ solar wind particles with an energy of 1 keV that we launched from the magnetopause with an isotropic velocity distribution and flux equal to the one considered by Killen et al. (2001). We found that 4×10^{26} H^+/s reach the surface for an IMF $(0,0,-14\ \mathrm{nT})$ and 2×10^{26} H^+/s reach the surface in the case of an IMF$(0,0,14\ \mathrm{nT})$. These values are 2–10 times smaller than the estimate of Killen et al. (2001) but can be considered as in agreement with their results since the results there highly depend on the magnetosphere model used to get these results. However, we can conclude that in our case we used magnetosphere model which is much less favorable to solar particle penetration than the model used by Killen et al. (2001).

2.6. Lifetime of the SEP inside the magnetosphere

For one observation of an energetic electrons burst by Mariner 10, a significant 6 seconds periodic variation of the flux was reported (Simpson et al., 1974). Baker et al. (1986) suggested that an electron burst was originally accelerated by a substorm phenomena (Siscoe et al., 1975), then injected inside close magnetic field lines near Mercury's surface, moved equatorially mirroring around Mercury in an azimuthal motion and was regularly and partially released when these particles were passing through region of open magnetic field lines of the magnetosphere. Luhmann et al.

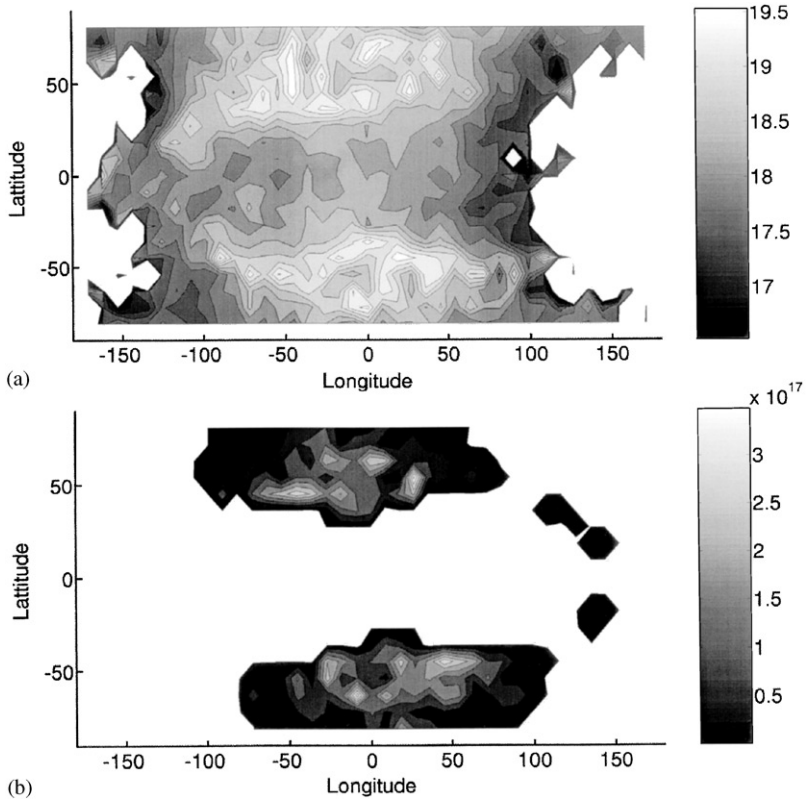

Fig. 4. Flux of keV/cm^2/s impacting Mercury's surface. (a) Log10 of the flux of H^+ ion. (b) Flux of electron. The subsolar point is placed in the center of each figure.

(1998) showed later that the regions of open magnetic field line could significantly change with IMF orientation, perhaps leading somehow to the electron bursts at times of IMF rotations or when new regions of the magnetosphere become open, releasing quasitrapped electrons. However, Ip (1987) underlined that such electrons were not able to remain inside Mercury's magnetosphere for the time suggested by Baker et al. (1986) mainly because of the gradient B drift effect. In the same way as suggested by Baker et al. (1986), SEP injected inside Mercury's magnetosphere could constitute a quasi-trapped population inside closed field lines trapped long enough to be at the origin of these bursts observed by Mariner 10 during hours.

Fig. 5a displays the total number of ions of each species remaining inside the magnetosphere following an instantaneous injection of energetic particles with an initial energy distribution shown in Fig. 1a. After an initial abrupt decrease (in less than 10 s the number of ions for each species inside the magnetosphere decreases by two orders of magnitude), the total number of ions inside the magnetosphere follows a much slower decrease (by one order in more than 60 s). The profiles shown in Fig. 5a are stopped after 70 s because of the limited number of test-particles used in our simulation. The almost flat shape of the profile above 40 s after injection indicates that a significant population of energetic ions should still be present inside the magnetosphere after a much longer time. As a comparison the azimuthal drift period of a 100 keV H^+ particle around Mercury is of the order of 1 s. Roughly 1 h after injection, a decrease by 10^6 of the total number of ions initially injected inside the magnetosphere can be estimated from Fig. 5a. This would still represent for H^+, for example, 10^{20} quasi-trapped ions. The result for the other ion species (Fig. 5a) show that for species with roughly the same gyroperiod the total number of particles remaining inside Mercury's magnetosphere after an instantaneous initial injection decreases faster for the lighter species (He^{2+}, triangle solid line) than for the heavier ones (Fe^{12+}, star solid line).

Fig. 5b presents the same result for electrons (solid line). The average lifetime of electrons inside Mercury's magnetosphere is 5 times smaller that for ions. The subsequent slower decrease is about one order of magnitude every 10 min. As a comparison the azimuthal drift period of a 100 keV electron around Mercury is of the order of 0.1 s. Therefore, it appears difficult to maintain a population of quasi-trapped electrons inside such Mercury's magnetosphere, hours after injection that would be able to generate the 10^4–10^5 300 keV electrons/cm^2/s observed by Mariner 10 (Simpson et al., 1974) as suggested by Baker et al. (1986) and discussed by Ip (1987).

The main factor limiting the ability to maintain charged particles inside Mercury's magnetosphere is their ability to

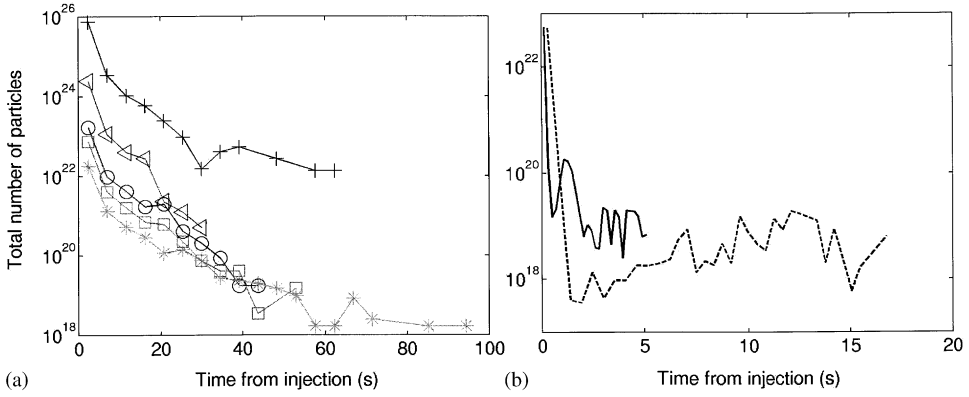

Fig. 5. Total number of particle inside Mercury's magnetosphere with respect to time after an instantaneous injection. The initial flux used are the ones presented in Fig. 1. (a) H^+ (solid cross line), He^{2+} (triangle solid line), C^{6+} (square solid line), O^{7+} (circle solid line) and Fe^{12+} (star solid line). (b) Electrons (solid line) and electrons inside a magnetosphere less compressed by the solar wind (dashed line).

move azimuthally inside closed field lines. This is strongly limited for the scaled version of the Earth's magnetosphere in which the ring current has been suppressed. The compression due to the solar wind also is a significant effect. Using a 7/5 larger version of the magnetosphere (with a spatial scale factor equal to 5 instead of 7), which corresponds to a 7/5 smaller solar pressure, the total number of electrons inside the magnetosphere after injection is plotted in Fig. 5b (dashed line). It was generated in the same way, and with a same number of initial test-particles, as the solid line. The total number of electron after the initial rapid decrease is much more larger than in the case of a more compressed magnetosphere (Fig. 5b). As shown in the next section, the choice of another IMF orientation also increases significantly the electron lifetime inside Mercury's magnetosphere.

2.7. *Effects of the interplanetary magnetic field*

Luhmann et al. (1998) showed the high variability of Mercury's magnetosphere with respect to the orientation of the IMF. In particular they showed that a positive Bz reduces considerably the surface of open magnetic field lines as compared to a negative Bz. This result was later confirmed by several authors (Killen et al., 2001; Kabin et al., 2000; Sarrantos et al., 2001). In this section, we present the dependence of the total flux impacting the surface with respect to the orientation of the IMF. We study three cases of IMF orientation at Mercury's orbit:

- an IMF $(0, 0, -14$ nT) where the surface is the less protected from incident solar particles,
- an IMF $(0, 0, 14$ nT) where the surface is the most protected from incident solar particles,
- an IMF $(0, -10, -10$ nT) used in the previous sections.

For these three case, Mercury's magnetosphere is calculated as in Luhmann et al. (1998). The method described in the previous sections to calculate the flux reaching the surface is then applied. We launched for each IMF orientation and for each ion species $\sim 400,000$ test-particles from the magnetopause with a truncated isotropic initial velocity distribution (same as in section 2.2) and followed them inside the magnetosphere until they either leave the magnetosphere or reach the surface. Each test-particle is weighted by a value calculated as described in Section 2.2 for the same initial flux (Fig. 1).

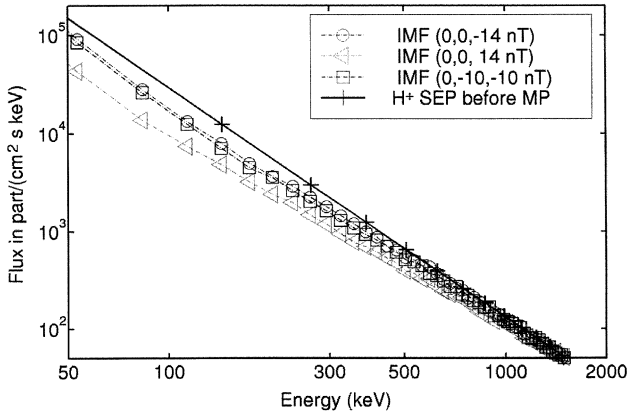

Fig. 6. Flux of impacting H^+ particles at Mercury's surface with respect to energy. Different cases of Mercury's magnetosphere corresponding to different cases of IMF are represented. Solid cross line: initial flux at the magnetopause (same as in Fig. 1a).

Fig. 6 provides the initial flux of SEP H^+ with respect to energy at the magnetopause (cross solid line) and the flux of H^+ particles impacting the surface for the three cases of IMF orientation. There is a significant variation of the total flux reaching the surface. Indeed from the case with an IMF (0,0,14 nT) in triangle dashed line to the case with an IMF $(0, 0, -14$ nT) in circle dashed line, the total flux of H^+ impacting the surface with an energy between 50 and 600 keV is multiplied by a factor 2. An IMF equal to $(0, -10, -10$ nT) or to $(0, 0, -14$ nT) leads to very similar total flux of H^+ impacting particle with respect to energy at

the surface. These calculations show that the sign of the Bz component of the IMF changes significantly the ability of energetic solar particles to reach the surface. Fig. 6 shows that above 1500 keV H^+ energy, solar H^+ ions are not significantly affected by the presence of Mercury's magnetosphere whatever is the IMF orientation. This also applies to the electrons and the other ions. That is, no change in the flux of impacting particles for energies above 2000 keV for He^{2+} ions, above 5000 keV for C^{6+}, O^{7+} and Fe^{12+} ions and above 200 keV for the electrons.

If a negative Bz IMF component opens the magnetosphere more than a positive Bz IMF component, it allows also quasi-trapped particles inside the magnetosphere to escape more easily. Fig. 7a compares the variation of the total number of H^+ particles inside the magnetosphere with respect to time after an instantaneous injection for two cases of IMF orientation. Fig. 7a has been obtained in the same way as Fig. 5a and should be compared to the solid cross line, the result for an IMF $(0,-10,-10$ nT). Of the initial $\sim 400,000$ incident H^+ test-particles, twice as many remain after 60 s for a positive Bz component, IMF $(0,0,14$ nT) (triangle solid line), than for a negative IMF Bz component, IMF $(0,0,-14$ nT) (cross solid line). This trend is also seen for all the species. For an IMF $(0,0,14$ nT), we find that He^{2+}, C^{6+}, O^{7+} and Fe^{12+} are still present inside Mercury's magnetosphere 75, 100, 90 and 95 s, respectively after injection. Quasi-trapped solar energetic electrons have significantly different lifetimes inside Mercury's magnetosphere for the different orientations (Fig. 7b). The total number of electron inside the magnetosphere decreases significantly slower in the case of an IMF (0,0,14 nT) than in the case of an IMF $(0,0,-14$ nT). Fig. 7b has been obtained for the same number of test-particles than for the results shown Fig. 5b. In the case of an IMF (0,0,14 nT) and a 7/5 less compressed magnetosphere, the total number of electrons remaining inside Mercury's magnetosphere decreases up to 5 times slower than in the case of a negative Bz IMF component and a more compressed Mercury's magnetosphere (Fig. 5b solid cross line). A quasi-trapped population of energetic electrons could be, therefore, maintained inside Mercury's magnetosphere for hours after an initial injection (with roughly a decrease by one order of magnitude of this total number every hour) if particular IMF and solar wind conditions prevail during this time interval.

The spatial distribution of impacts is also dependent on the IMF orientation. Fig. 8a presents the impacting flux of H^+ particles at the surface for an IMF equal to $(0,0,-14$ nT) whereas Fig. 8b presents the same flux but for an IMF equal to (0,0,14 nT). As for Fig. 4a (obtained for an IMF $(0,-10,-10$ nT)), the initial SEP H^+ flux at the magnetopause is the one provided in Fig. 1a. The same method and number of test-particle have been used to calculate the results provided in the three figures. Fig. 8 shows symmetric profiles with respect to the equator (in the limit of statistical noise due to the use of a limited number of test-particle). Fig. 8a presents a more distributed flux with respect to latitude than Fig. 8b. This can be explained by the fact that the larger volume of open magnetic field lines in the case of an IMF $(0,0,-14$ nT) allows impacting particles to reach a larger area on the surface than in the case of an IMF $(0,0,14$ nT). The scale bars on the right side of each figure indicate that the total flux for an IMF $(0,0,-14$ nT) is larger than for the case of an IMF (0,0,14 nT) as shown in Fig. 6. The main difference between Figs. 8a and 4a is the non-zero value of the IMF By component for the result in Fig. 4a. In such a case, we obtained a slight but significant asymmetry with respect to the equator (Killen et al., 2001; Sarrantos et al., 2001). Indeed a non-zero By component introduces a north/south asymmetry which could be at the origin of the north/south asymmetry of the exospheric sodium emission observed by Potter and Morgan (1990, 1997) and Potter et al. (1999). Same results are obtained for the other ion species and electron.

2.8. *Sputtering of sodium atoms from the surface*

Potter et al. (1999) reported an observation in which the total sodium atom content of Mercury's exosphere increased by a factor three in less than 8 Earth days, which is less than 1/7 of one Mercury's day. Such an increase is difficult to relate to the variation of Mercury's position with respect to the Sun or to a change in the solar photon flux. It is much more likely to be explained by a variation in Mercury's plasma environment. When Potter et al. (1999) described their observation, they suggested that it might be related to the encounter between Mercury and SEP events (GPE-type events). Later Killen et al. (2001) suggested that this observation could be explained by the variation of the solar wind flux intensity and by the change of the IMF orientation. In this section, we estimate whether or not the SEP event studied here could produce the $\sim 10^{28}$ Na atoms in Mercury's exosphere suggested by the observations of Potter et al. (1999).

In previous sections, the flux of ions impacting Mercury's surface for three different IMF orientations was presented. These energetic ions and electrons can enhance the sodium exosphere content in two ways (McGrath et al., 1986). They can directly sputter the available surface sodium atoms or they can enhance diffusion of sodium atoms to the surface, where it is subsequently ejected by photo stimulated or thermal desorptions. Here, we use the flux to the surface to estimate the total number of sodium atoms sputtered. The efficiency of a particle to eject sodium atoms from a surface is highly dependent on its velocity when it impacts the surface, on its nuclear charge or mass, and on the sodium atoms concentration and porosity of the surface. In Fig. 9 we give estimates of the yield vs. impact energy for the five ion species. The yield, Y_{Na}, is defined as the number of sodium atoms ejected from the surface by an impacting particle. Incident fast ions and electrons do not efficiently sputter by knock-on collisions. They primarily

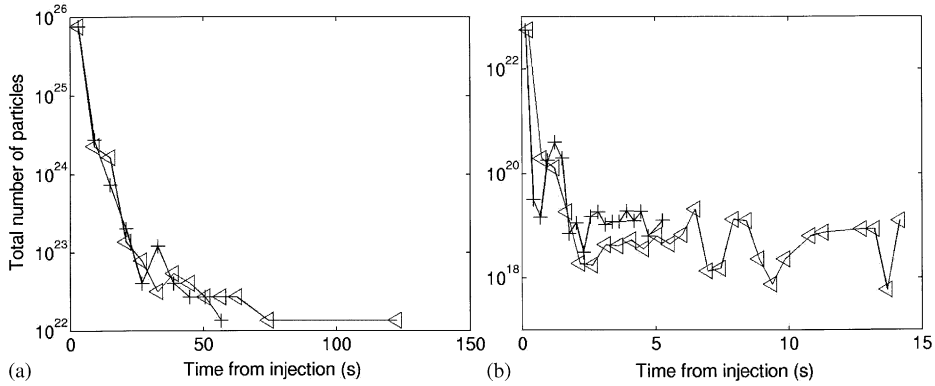

Fig. 7. Number of particles inside Mercury's magnetosphere with respect to time after an instantaneous injection at the magnetopause. (a) H^+ ions. (b) Electrons. Cross solid line: IMF(0,0,14 nT). Triangle solid line: IMF$(0,0,-14$ nT).

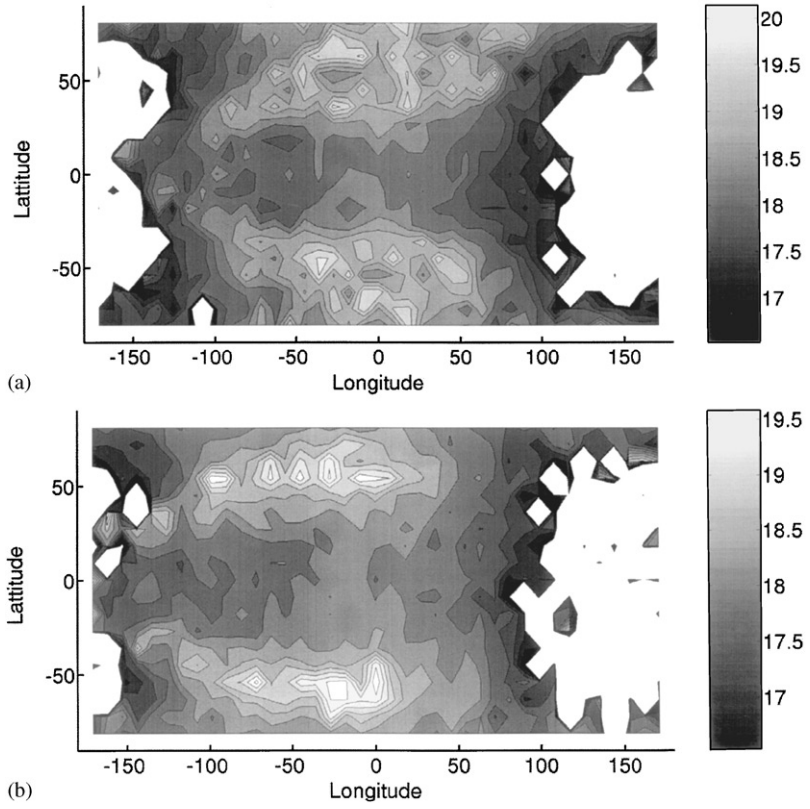

Fig. 8. Log10 of the flux of H^+ in keV/cm^2/s impacting Mercury's surface. (a) For an IMF vector equal to $(0,0,-14$ nT). (b) For an IMF vector equal to (0,0,14 nT). The subsolar point is placed in the center of each figure.

lose their energy in a solid by ionization and excitation, producing a cascade of low energy electrons. The number of electron produced per unit path length near the surface is $\sim (\mathrm{d}E/\mathrm{d}x)_e/W$, where $\sim (\mathrm{d}E/\mathrm{d}x)_e$ is the mean electronic energy loss per unit path length in the solid and W is the average energy required to produce a secondary electron, a tabulated quantity. The shower of electrons so produced can then lead to desorption of sodium atoms. Using sodium atom desorption cross-sections, σ_d, measured for low energy electrons (< 100 eV) (Yakshinskiy and Madey, 1999) and a mean transport length, λ, for the secondary electrons, then $Y_{Na} \simeq \bar{f}[\lambda(\mathrm{d}E/\mathrm{d}x)_e/W]\sigma_d N_{Na}$. Here N_{Na} is the surface density (atoms/area) of sodium atoms and $\bar{f}$ a correction factor. This factor accounts for averaging $(\mathrm{d}E/\mathrm{d}x)_e$ over incident angle and porosity. $(\mathrm{d}E/\mathrm{d}x)_e$ for the ions was obtained using TRIM software (Ziegler et al., 1985) for a SiO_2 grains. A surface density equal to $\sim 3\times10^{13}$ Na/cm^2 was used corresponding to a bulk concentration of ~ 0.003. Although sodium atoms do not stick efficiently at the dayside temperatures of Mercury, we set $\bar{f} \sim 1$ allowing the

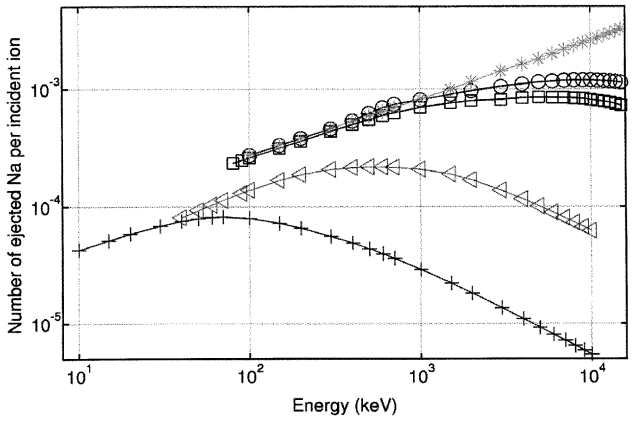

Fig. 9. Number of ejected sodium atoms from Mercury's surface with respect to the energy of the impacting ion (TRIM, Ziegler et al., 1985). Solid cross line: H^+ impacting Mercury's surface. Solid triangle line: He^{2+} impacting Mercury's surface. Solid square line: C^{6+} impacting Mercury's surface. Solid circle line: O^{7+} impacting Mercury's surface. Solid star line: Fe^{12+} impacting Mercury's surface.

porosity to cancel the enhancement for angular incidence, giving a conservative lower bond (Johnson, 1990). Using a mean secondary electron energy $\sim$ 30 eV, then $\sigma_d \simeq 10^{-19}$ cm^2. Whereas the incident ions are likely highly charged, the resulting yields, given in Fig. 9 are for equilibrium charge state ions consistent with a firm lower bound. To account for the angular incidence, a factor $\sim$ 2 times the value at normal incidence is needed.

For electronic sputtering by energetic SEP ions we found yields between 10^{-2} and 10^{-5} as given in Fig. 9, assuming the surface concentration above. Using these we calculated the total number of sodium atoms ejected at the surface of Mercury per second by the ions reaching the surface. Fig. 10 presents the distribution of the total flux of sodium atoms ejected from Mercury's surface (in Na/s) in the case of an IMF equal to $(0, -10, -10$ nT) and an intitial SEP flux presented in Fig. 1. As can be seen in Fig. 10, a strong dawn/dusk asymmetry of the sodium atoms ejected from the surface is produced by such SEP but also a slight north/south asymmetry due to the By non-zero component as explained in Section 3.3. These results have been obtained by supposing a uniform and steady concentration of sodium atoms at the surface. This assumption is probably not accurate because sodium atoms density should be larger on the dawn side than on the dusk side (Hunten and Sprague, 2002; Leblanc and Johnson, 2003). Indeed thermal desorption ejects sodium atoms from the surface very efficiently as soon as the surface reaches a temperature of 400 K. Moreover the sticking property of sodium atoms on a surface is highly dependent on the temperature (Yakshinskiy and Madey, 2000). A sodium atom ejected from Mercury's surface would then preferentially migrate towards cold regions, that is towards the nightside (Hunten and Sprague, 2002) and the poles. This results in a rapid depletion of sodium atoms in the surface as soon as this surface reaches a temperature above 400 K, that is, in the early morning (Leblanc and Johnson, 2003). Moreover, enrichment of sodium atoms of the surface by micro-meteoritic bombardment is higher at the dawn side than at the dusk side (Killen and Ip, 1999). All these reasons tend to create an initial dawn/dusk asymmetry of sodium atom concentration inside the surface which would increase the asymmetry due to SEP bombardment (Fig. 10).

Integrating over the whole surface, we obtain that a total of 6×10^{20} Na/s are sputtered from the surface by the total flux of SEP impacting the surface in the case of an IMF $(0, -10, -10$ nT) whereas for an IMF equal to $(0, 0, -14$ nT), 6×10^{20} Na/s are ejected inside the exosphere and for an IMF $(0, 0, 14$ nT) 3×10^{20} Na/s. If we consider that the lifetime of such sodium atoms against ionization at Mercury's orbital distance to the Sun is equal to $\sim 10^4$ s, the encounter of the SEP event, shown in Fig. 1, would enrich Mercury's exosphere by $\sim 10^{25}$ Na. The H^+ ions generate $\sim$ 90% of the sodium atoms ejected, whereas SEP He^{2+} contributes to $\sim$ 6%, O^{7+} to $\sim$ 2%, and C^{6+} and Fe^{12+} to $\sim$ 1% each. Indeed SEP H^+ flux impacting the surface, 8×10^{24} H^+/s, is one to two orders larger than the ones of the other ion species: 3×10^{23} He^{2+}/s, 2×10^{22} O^{7+}/s, 8×10^{21} C^{6+}/s and 2×10^{21} Fe^{12+}/s. The electrons only poorly contribute to the total atmosphere and only at high latitudes (Fig. 4b) because their flux is much less intense (Fig. 1b) and because their efficiency to eject sodium atoms from the surface is less than that for the ions.

The contribution to the exosphere, $\sim 10^{25}$ Na, due to an event with intensities of the order of those in Fig. 1 is three orders of magnitude less that what is needed, 10^{28} Na, to produce the variations of the total sodium atom content of Mercury's exosphere observed by Potter et al. (1999). Based on these lower bounds, an IFE event is an unlikely source. Indeed, their flux is usually much smaller than that associated with a GPE (Reames, 1999). Mason et al. (1999) reported a GPE event observed by Advanced Composition Explorer (ACE) that occurred only 10 days (November 4 1997) before the observations (13–20th, Potter et al., 1999). ACE measured flux intensities three orders larger than the flux intensities used in this work. Moreover, we considered only the part of a SEP event which would reach Mercury before or few hours after the arrival at Mercury of the shock and magnetic cloud usually associated with a GPE. When a shock and magnetic cloud are observed, a significant intensity enhancement occurs (Reames et al., 1997b). This would correspond to a significant enhancement of the flux to Mercury's surface and to a corresponding enhancement in the quantity of sodium ejected. However, the time length of this peak of SEP flux intensity is much shorter (only few hours) than the 8 Earth days during which the increase of the sodium atom content inside Mercury's exosphere was observed by Potter et al. (1999). Therefore such encounter, in order to reproduce Potter et al. (1999) observations, would have to eject from the surface such an amount of sodium atoms that

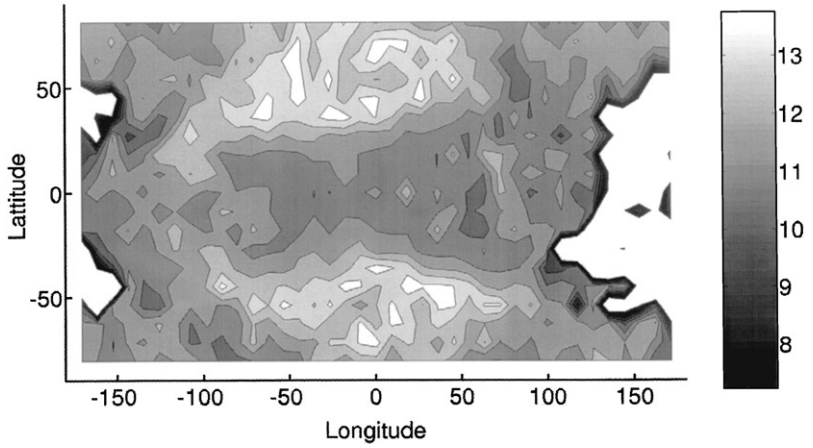

Fig. 10. Total flux in Na/s ejected from Mercury's surface in the case of Mercury magnetosphere with an IMF $(0, -10, -10$ nT). The subsolar point is placed in the center of the figure.

could be preserved for several ionization times. Actually , in such a case, several successive GPE should be involved to fit Potter et al. (1999) observations as these authors suggested it. Moreover the shock and its peak intensity should significantly compress Mercury's magnetosphere. This would increase the surface bombarded by a SEP event, but also it should suppress the usual high latitude concentrations of the impacting flux. Actually, the observations of Potter et al. (1999) show during the first 4 days of the observations a peak of emission significantly concentrated at the north hemisphere (corresponding to the situation described in this work for a strong non-zero By component with respect to the other B components). During the last 3 days of the observations the emission peak was much closer to the equator and was distributed symmetrically with respect to it.

3. Conclusion

Potter et al. (1999) observed an increase of the total content of sodium inside Mercury's exosphere by a factor three in less than 8 Earth days. Such an increase is difficult to explain by the variation of Mercury's position with respect to the Sun. It is more likely to be related to variations of Mercury's plasma environment. Moreover the asymmetry of the emission with respect to the equator showing significant peaks of emission concentrated, at least at the beginning of the observation, at high latitudes suggests that this enhancement is probably related to solar particles penetrating the magnetosphere through open magnetic field lines and impacting the surface. These authors proposed that the encounter of Mercury with coronal mass ejection (CME) events could cause such an enhancement. Killen et al. (2001) more recently suggested that this variation was due to strong variations of the solar wind flux and to IMF orientation changes.

In this work we describe the effects of a solar energetic particle (SEP) event encountering Mercury, including IMF orientation effects on SEP access to the magnetosphere and surface. We consider a particular SEP event measured in detail at the Earth (Reames et al., 1997a) and rescale it to Mercury's orbit. This study is limited to the particles (> 10 keV/amu) which would reach Mercury before or few hours after the arrival of the shock and magnetic cloud usually associated with a CME that is for an unperturbated Mercury's magnetosphere for quiet solar wind conditions. Test-particles representative of the energy flux distribution for each SEP ion species and for the electrons are launched from the magnetopause and followed inside Mercury's magnetosphere model of Luhmann et al. (1998). The distribution of particles reaching the surface is then computed. These particles can cause electronically induced desorption of sodium atoms and, because they penetrate more than the solar wind ions or UV photons, they can enhance the supply of sodium atoms to the surface where it can be desorbed by thermal or photo stimulated desorptions.

The flux of SEP impacting Mercury's surface is highly asymmetric with respect to longitude with a significant larger flux of impacting particles at the dawn side than at the dusk side of the planet (Fig. 4). This asymmetry is suggestive of the dawn/dusk asymmetry of the sodium emission reported by Sprague et al. (1997). Significant peaks of intensity in the SEP flux reaching the surface at high latitudes might also be related to the enhancement reported by Potter and Morgan (1990) and Potter et al. (1999). The intensity of the impacting flux at the surface varies also with respect to the IMF orientation. Such dependence could lead to a variation of the total sputtered flux with respect to IMF orientation by a factor two.

Energetic particles penetrating Mercury's magnetosphere are at the origin of a quasi-trapped population of energetic electrons and ions which can persist inside Mercury's magnetosphere for hours after injection. The capacity of Mer-

cury's magnetosphere to capture an energetic particle is highly dependent on the IMF orientation and on the solar wind pressure but also on the unknown structure of the magnetic field close to the planet. The observations by Mariner 10 of energetic fluxes of electrons (Simpson et al., 1974) could, therefore, be due to solar energetic particles trapped inside Mercury's magnetosphere before the arrival of Mariner 10 and released in relation with changes of the IMF orientation (Luhmann et al., 1998).

Using a rough lower bound to the yield, the particular SEP event (Reames et al., 1997a) used in this work does not appear intense enough to directly eject the total amount of sodium atoms needed to reproduce the observations of Potter et al. (1999). However, much stronger SEP events that the one used in this work have been observed at the Earth (Mason et al., 1999) during the same month as the Potter et al. (1999) observations and may have sufficient intensities. In addition, the energy deposited by the penetrating ions and electrons can enhance diffusion of sodium atoms to the surface layer (McGrath et al., 1986), where photo stimulated and thermal desorptions are efficient. Although the solar wind flux variations suggested by Killen et al. (2001) could be the origin of these observations the geometry of the bombardment in Fig. 4 is suggestive. Therefore, it is still possible that Potter et al. (1999) observed the product of the encounter of a strong SEP event (with at least flux of 10^9 $H^+/(cm^2$ sr MeV) at 0.1 MeV) with Mercury.

Also, SEP events may constitute a regular source of variability of Mercury's exosphere, especially at solar maximum. It would be interesting to examine archives of observations of sodium brightenings to see if there is indication of a SEP event or solar cycle relationship. These results are also pertinent to future measurements on the Messenger and Bepi Colombo missions, which will be instrumented to observe both the exosphere and the local particles and fields.

Acknowledgements

The work at the University of Virginia was supported by the NSF Astronomy Division and by NASA's Planetary Atmospheres Program.

References

Baker, D.N., 1986. Jovian electron populations in the magnetosphere of Mercury. Geophys. Res. Lett. 13, 789.

Baker, D.N., Simpson, J.A., Eraker, J.H., 1986. A model of impulsive acceleration and transport of energetic particles in Mercury's magnetosphere. J. Geophys. Res. 91, 8742.

Baring, M.G., Ogilvie, K.W., Ellison, D.C., Forsyth, R.J., 1997. Acceleration of solar wind ions by nearby interplanetary shocks: comparison of Monte Carlo simulation with Ulysses observations. Astrophys. J. 476, 889.

Bida, T.A., Killen, R.M., Morgan, T.H., 2000. Discovery of calcium in Mercury's atmosphere. Nature 404, 159.

Brecht, S.H., 1997. Solar wind proton deposition into the Martian atmosphere. J. Geophys. Res. 102, 11287.

Broadfoot, A.L., Shemansky, D.E., Kumar, S., 1976. Mariner 10: Mercury atmosphere. Geophys. Res. Lett. 3, 577.

Burlaga, L.F.E., 1991. Magnetic clouds. In: Schwenn R., Marsch, E. (Eds.), Physics of the Inner Heliosphere II. Springer, Berlin, Heidelberg.

Cintala, M.J., 1992. Impact-induced thermal effects in the lunar and Mercurian regolith. J. Geophys. Res. 97, 947.

Delcourt, D.C., Moore, T.E., Orsini, S., Millilo, A., Sauvaud, J.-A., 2002. Centrifugal acceleration of ions near Mercury. Geophys. Res. Lett. 29 (12), 1591, 10.1029/2001GL013829.

Delcourt, D.C., Grimald, S., Leblanc, F., Bertherlier, J.-J., Millilo, A., Mura, A., 2003. A quantitative model of planetary Na^+ contribution to Mercury's magnetosphere. Ann. Geophys., submitted for publication.

Ellison, D.C., Ramaty, R., 1985. Shock acceleration of electrons and ions in solar flares. Astrophys. J. 298, 400.

Eraker, J.H., Simpson, J.A., 1986. Acceleration of charged particles in Mercury's magnetosphere. J. Geophys. Res. 91, 9973.

Goldstein, B.E., Suess, S.T., Walker, R.J., 1981. Mercury: Magnetospheric Processes and the Atmospheric supply and loss rates. J. Geophys. Res. 86, 5485.

Gosling, J.T., Asbridge, J.R., Bame, S.J., Feldman, W.C., Zwickl, R.D., Paschmann, G., Skopke, N., Hynds, R.J., 1981. Interplanetary ions during an energetic storm particle event: the distribution function from solar wind thermal energies to 1.6 MeV. J. Geophys. Res. 86, 547.

Hunten, D.M., Sprague, A.L., 1997. Origin and character of the lunar and Mercurian atmosphere. Adv. Space Res. 19, 1551.

Hunten, D.M., Sprague, A.L., 2002. Diurnal variation of Na and K at Mercury. Meteoritic Planet. Sci. 37, 1165.

Hunten, D.M., Morgan, T.H., Shemansky, D.E., 1988. The Mercury atmosphere. In: Vilas, F., Chapman, C.R., Matthews, M.S. (Eds.), Mercury. University of Arizona Press, Tucson.

Ip, W.-H., 1987. Dynamics of electrons and heavy ions in Mercury's magnetosphere. Icarus 71, 441.

Ip, W.-H., 1993. On the surface sputtering effects of magnetospheric charged particles at Mercury. Astrophys. J. 418, 451.

Johnson, R.E., 1990. Energetic charged-particle interactions with atmospheres and surfaces, Springer-Verlag, Berlin.

Kabin, K., Gombosi, T.I., DeZeeuw, D.L., Powell, K.G., 2000. Interaction of Mercury with the solar wind. Icarus 143, 397.

Kahler, S.W., Sheeley Jr., N.R., Howard, R.A., Koomen, M.J., Michels, D.J., McGuire, R.E., Von Rosenvinge, T.T., Reames, D.V., 1984. Associations between coronal mass ejections and solar energetic proton events. J. Geophys. Res. 89, 9683.

Killen, R.M., Ip, W.-H., 1999. The surface bounded atmosphere of Mercury and the Moon. Rev. Geophys. 37, 361.

Killen, R.M., Potter, A.E., Reiff, P., Sarantos, M., Jackson, B.V., Hick, P., Giles, B., 2001. Evidence for space weather at Mercury. J. Geophys. Res. 106, 20 509.

Langevin, Y., 1997. The regolith of Mercury: present knowledge and implications for the Mercury orbiter mission. Planet. Space Sci. 45, 31.

Leblanc, F., Johnson, R.E., 2003. Mercury's sodium exosphere. Icarus, submitted for publication.

Leblanc, F., Luhmann, J.G., Johnson, R.E., Chassefière, E., 2002. Some expected impacts of a solar energetic particle event at Mars. J. Geophys. Res. 107, 10.1029/2001JA900178.

Lee, M.A., 1997. Particle acceleration and transport at CME driven shocks. In: Crooker, N., Joselyn, J.A., Feynman, J. (Eds.), Coronal Mass Ejection. Geophysical Monograph 99, AGU, 227.

Luhmann, J.G., Russell, C.T., Tsyganenko, N.A., 1998. Disturbances in Mercury's magnetosphere: are the mariner 10 "substorms" simply driven?. J. Geophys. Res. 103, 9113.

Luhmann, J.G., Acuña, M.H., Purucker, M., Russell, C.T., Lyon, J.G., 2002. The martian magnetosheath: how Venus-like?. Planet. Space Sci. 50, 489.

Madey, T.E., Yakshinskiy, B.V., Ageev, V.N., Johnson, R.E., 1998. Desorption of alkali atoms and ions from oxide surfaces: relevance to origins of Na and K in atmospheres of Mercury and the Moon. J. Geophys. Res. 103, 5873.

Mason, G.L., et al., 1999. Particle acceleration and sources in the November 1997 solar energetic particle event. Geophys. Res. Lett. 26, 141.

McGrath, M.A., Johnson, R.E., Lanzerotti, L.J., 1986. Sputtering of sodium on the planet Mercury. Nature 323, 694.

Morgan, T.H., Zook, H.A., Potter, A.E., 1988. Impact-driven supply of sodium and potassium to the atmosphere of Mercury. Icarus 75, 156.

Ness, N.F., Behannon, K.W., Lepping, R.P., Whang, Y.C., Shatten, K.H., 1974. Magnetic field observations near Mercury: preliminary results from Mariner 10. Science 185, 151.

Oetlicker, M., Klecker, B., Hovestadt, D., Mason, G.M., Mazur, J.E., Leske, R.A., Mewaldt, R.A., Blake, J.B., Looper, M.D., 1997. The ionic charge of solar energetic particles with energies of 0.3–70 MeV per nucleon. Astrophys. J. 477, 495.

Ogilvie, K.W., Scudder, J.D., Vasyliunad, V.M., Hartle, R.E., Siscoe, G.L., 1977. Observations at the planet Mercury by the plasma electron experiment: Mariner 10. J. Geophys. Res. 82, 1807.

Potter, A.E., 1995. Chemical sputtering could produce sodium vapor and ice on Mercury. Geophys. Res. Lett. 22, 3289.

Potter, A.E., Morgan, T.H., 1985. Discovery of sodium in the atmosphere of Mercury. Science 229, 651.

Potter, A.E., Morgan, T.H., 1986. Potassium in the atmosphere of Mercury. Icarus 67, 336.

Potter, A.E., Morgan, T.H., 1987. Variation of sodium on Mercury with solar radiation pressure. Icarus 71, 472.

Potter, A.E., Morgan, T.H., 1990. Evidence for magnetospheric effects on the sodium atmosphere of Mercury. Science 248, 835.

Potter, A.E., Morgan, T.H., 1997. Evidence of suprathermal sodium on Mercury. Adv. Space Res. 19, 1571.

Potter, A.E., Morgan, T.H., Killen, R.M., 1999. Rapid changes in the sodium exosphere of Mercury. Planet. Space Sci. 47, 1441.

Reames, D.V., 1995. Solar energetic particles: a paradigm shift. Rev. Geophys. 30, 585.

Reames, D.V., 1999. Particle acceleration at the sun and in the heliosphere. Space Sci. Rev. 413, 413.

Reames, D.V., Barbier, L.M., von Rosenvinge, T.T., Mason, G.M., Mazur, J.E., Dwyer, J.R., 1997a. Energy spectra of ions accelerated in impulsive and gradual solar events. Astrophys. J. 483, 515.

Reames, D.V., Kahler, S.W., Ng, C.K., 1997b. Spatial and temporal invariance in the spectra of energetic particles in gradual solar events. Astrophys. J. 491, 414.

Sarrantos, M., Reiff, P.H., Hill, T.W., Killen, R.M., Urquhart, A.L., 2001. A bx-interconnected magnetosphere model for Mercury. Planet. Space Sci. 49, 1629.

Shemansky, D.E., Broadfoot, A.L., 1977. Interaction of the surfaces of the Moon and Mercury with their exospheric atmospheres. Rev. Geophys. 15, 491.

Simnett, G.M., 1974. Relativistic electron events in interplanetary space. Space Sci. Rev. 16, 257.

Simpson, J.A., Eraker, J.H., Lamport, J.E., Walpole, P.H., 1974. Electrons and protons accelerated in Mercury's magnetic field. Science 185, 160.

Siscoe, G.L., Ness, N.F., Yeates, M., 1975. Substorms on Mercury? J. Geophys. Res. 80, 4359.

Smyth, W.H., 1986. Nature and variability of Mercury's sodium atmosphere. Nature 323, 696.

Sprague, A.L., Kozlowski, R.W.H., Hunten, D.M., 1997. Distribution and abundance of sodium in Mercury's atmosphere, 1985–1988. Icarus 129, 506.

Tsyganenko, N.A., 1996. Effects of the solar wind conditions on the global magnetospheric configuration as deduced form databased models. In: Proceeding of Third International Conference on Substorms (ICS-3). Eur. Space Agency Spec. Publ. ESA SP389, 181.

Tylka, A.J., 2001. New insights on solar energetic particles from Wind and ACE. J. Geophys. Res. 106, 25333.

Von Steiger, R., Schwadron, N.A., Fisk, L.A., Geiss, J., Gloecker, G., Hefti, S., Wilken, B., Wimmer-Schweingruber, R.F., Zurbuchen, T.H., 2000. Composition of quasi-stationary solar wind flows from Ulysses/solar wind ion composition spectrometer. J. Geophys. Res. 105, 27217.

Yakshinskiy, B.V., Madey, T.E., 1999. Photon-stimulated desorption as a substantial source of sodium in the lunar atmosphere. Nature 400, 642.

Yakshinskiy, B.V., Madey, T.E., 2000. Thermal desorption of sodium atoms from thin SiO_2 films. Surf. Rev. Lett. 7, 75.

Ziegler, J.F., Biersack, J.P., Littmark, V., 1985. The Stopping and Ranges of Ions in Solids. Pergamon Press, New York.